THE JOURNAL OF PHYSICAL CHEMISTRY B

Article

Water Concentration Profiles in Membranes Measured by ESEEM of Spin-Labeled Lipids

Denis A. Erilov, Rosa Bartucci, Rita Guzzi, Alexander A. Shubin, Alexander G. Maryasov, Derek Marsh, Sergei A. Dzuba, and Luigi Sportelli

J. Phys. Chem. B, **2005**, 109 (24), 12003-12013• DOI: 10.1021/jp050886z • Publication Date (Web): 28 May 2005

Water Concentration Profiles in Membranes Measured by ESEEM of Spin-Labeled Lipids

Denis A. Erilov,[†,‡] Rosa Bartucci,*[,†] Rita Guzzi,[†] Alexander A. Shubin,[⊥] Alexander G. Maryasov,[||] Derek Marsh,[§] Sergei A. Dzuba,[||] and Luigi Sportelli[†]

Dipartimento di Fisica and Unità INFM, Università della Calabria, I-87036 Arcavacata di Rende (CS), Italy, Department of Physics, Novosibirsk State University, 630090 Novosibirsk, Russian Federation, Max-Planck-Institut fur Biophysikalische Chemie, Abteilung Spektroskopie, 37077 Göttingen, Germany, and Institute of Chemical Kinetics and Combustion and Boreskov Institute of Catalysis, Russian Academy of Science, 630090 Novosibirsk, Russian Federation

Received: February 21, 2005; In Final Form: April 22, 2005

Electron spin−echo envelope modulation (ESEEM) spectroscopy of phospholipids spin-labeled systematically down the *sn*-2 chain was used to detect the penetration of water (D_2O) into bilayer membranes of dipalmitoyl phosphatidylcholine with and without 50 mol % cholesterol. Three-pulse stimulated echoes allow the resolution of two superimposed ^{2}H-ESEEM spectral components of different widths, for spin labels located in the upper part of the lipid chains. Quantum chemical calculations (DFT) and ESEEM simulations assign the broad spectral component to one or two D_2O molecules that are directly hydrogen bonded to the N−O group of the spin label. Classical ESEEM simulations establish that the narrow spectral component arises from nonbonded water (D_2O) molecules that are free in the hydrocarbon chain region of the bilayer membrane. The amplitudes of the broad ^{2}H-ESEEM spectral component correlate directly with those of the narrow component for spin labels at different positions down the lipid chain, reflecting the local H-bonding equilibria. The D_2O-ESEEM amplitudes decrease with position down the chain toward the bilayer center, displaying a sigmoidal dependence on position that is characteristic of transmembrane polarity profiles established by other less direct spin-labeling methods. The midpoint of the sigmoidal profile is shifted toward the membrane center for membranes without cholesterol, relative to those with cholesterol, and the D_2O-ESEEM amplitude in the outer regions of the chain is greater in the presence of cholesterol than in its absence. For both membrane types, the D_2O amplitude is almost vanishingly small at the bilayer center. The water-penetration profiles reverse correlate with the lipid-chain packing density, as reflected by ^{1}H-ESEEM intensities from protons of the membrane matrix. An analysis of the H-bonding equilibria provides essential information on the binding of water molecules to H-bond acceptors within the hydrophobic interior of membranes. For membranes containing cholesterol, approximately 40% of the nitroxides in the region adjacent to the lipid headgroups are H bonded to water, of which ca. 15% are doubly H bonded. Corresponding H-bonded populations in membranes without cholesterol are ca. 20%, of which ca. 6% are doubly bonded.

Introduction

The bilayer lipid membrane demarcates the outer boundary of biological cells and their internal organelles. It constitutes the permeability barrier that distinguishes the external environment from the internal compartments. Not only is the interaction of water with the lipid bilayer fundamental to the formation and stability of biological membranes (e.g., ref 1), but also the partial penetration of water into the lipid interior gives rise to the characteristic shape of the hydrophobic membrane barrier.[2] The latter is an important energetic determinant for the insertion of proteins, peptides, and lipid amphiphiles into the membrane and also for the permeation of polar solutes across the membrane.

Continuous-wave (CW) electron-spin resonance (ESR) methods that employ site-directed spin labeling of the lipid chains have been used to establish the transmembrane polarity profile of lipid bilayers in varying degrees of detail.[2−5] High-resolution profiles reveal a sigmoidal, troughlike dependence on chain position in which a transition takes place from a high-polarity region adjacent to the lipid headgroups to a low-polarity region at the center of the membrane.[4] The position, width, and magnitude of the transition region depend on the membrane lipid composition, particularly on cholesterol content, and on the lipid phase.

CW-ESR determinations of membrane polarity are based on measurements of spin-labeled ^{14}N hyperfine splittings and g_{xx} values,[6] which depend additionally on the local dielectric constant. They reflect water penetration indirectly via the effects of hydrogen bonding on the quantum chemical properties of the nitroxide. Direct detection of water penetration into membranes is possible, however, by electron spin−echo spectroscopy, again using site-specifically spin-labeled lipid chains.[7−10] The strength of the modulation of the electron spin−echo decay (ESEEM) by deuterium hyperfine interactions with D_2O depends

* Corresponding author. E-mail: bartucci@fis.unical.it. Fax: +39 0984 49 44 01.
[†] Università della Calabria.
[‡] Novosibirsk State University.
[§] Max-Planck-Institut fur Biophysikalische Chemie.
[||] Institute of Chemical Kinetics and Combustion, Russian Academy of Science.
[⊥] Boreskov Institute of Catalysis, Russian Academy of Science.

10.1021/jp050886z CCC: $30.25
Published on Web 05/28/2005

not only on the distance from the spin label but also on the local concentration of D_2O water molecules.

All of the previously quoted ^{2}H-ESEEM measurements on D_2O penetration into membranes have concentrated on a restricted number of spin-labeled positions and, significantly, have used two-pulse echo techniques exclusively. With the latter, the resolution in the Fourier transform ESEEM spectrum (when performed) is seriously limited by the spin-labeled T_2 decay time. This problem can be overcome, however, by using three-pulse stimulated echoes.[11] In the present work, we have investigated the water penetration profiles into membranes with a complete range of spin-labeled positions and using three-pulse stimulated electron spin echoes. By this means, it is possible to resolve the ^{2}H-ESEEM spectral components from D_2O molecules both H bonded to the spin label and free within the hydrophobic membrane interior and to map out the water penetration profile at high spatial resolution. Additionally, the ^{1}H-ESEEM spectra from matrix protons bonded to the lipids are used to correlate water penetration with the packing density of the lipid chains.

Materials and Methods

Materials. Synthetic 1,2-dipalmitoyl-*sn*-glycero-3-phosphocholine (DPPC) and cholesterol were obtained from Sigma/Aldrich (St. Louis, MO). Phosphatidylcholines spin-labeled in the *sn*-2 chain (*n*-PCSL; 1-acyl-2-(*n*-doxyl)stearoyl-*sn*-glycero-3-phosphocholine) were synthesized according to Marsh and Watts.[12] Certain positional spin-labeled isomers were also obtained from Avanti Polar Lipids (Birmingham, AL). Reagent-grade salts for the 10 mM phosphate D_2O buffer solution at pH 7.5 were from Merck (Darmstadt, Germany). All materials were used as purchased with no further purification.

Sample Preparation. DPPC and 1 mol % *n*-PCSL, with and without 50 mol % cholesterol, were codissolved in chloroform. The solvent was evaporated in a nitrogen gas stream, and then residual traces of solvent were removed by drying under vacuum overnight. The lipids were dispersed at a concentration of ca. 100 mg/mL in pH 7.5 phosphate D_2O buffer by vortex mixing with heating to 60 °C (i.e., above the chain-melting transition of DPPC). The hydrated lipid bilayers were transferred to a standard 4-mm-diameter quartz ESR tube and concentrated by pelletization in a benchtop centrifuge, and then the excess buffer was removed. Samples were incubated for 24 h at 10 °C before measuring. All measurements were performed at liquid-nitrogen temperature, and samples were cooled slowly at approximately 3 °C/min.

EPR Spectroscopy. Data were collected on an ELEXSYS E580 9-GHz Fourier transform FT-EPR spectrometer (Bruker, Germany) equipped with an MD5 dielectric resonator and a CF 935P cryostat (Oxford Instruments, U.K.). Three-pulse stimulated echo ($^{\pi}/_2-\tau-^{\pi}/_2-T-^{\pi}/_2-\tau$ echo) decays were obtained by using a microwave pulse width of 12 ns, with the microwave power adjusted to give $^{\pi}/_2$ pulses. The time delay T between the second and the third pulses was incremented from 20 ns by 700 steps of 12 ns each while maintaining the separation τ between the first and the second pulses constant at 168 ns or 204 ns. A four-step phase-cycling program was used to eliminate unwanted echoes. The data were treated as follows: (1) the average experimental echo decay was fitted with a biexponential function; (2) the data were then divided by the fitted average decay function so that only oscillations about unity remained; (3) the unit level was subtracted from the signal; (4) zero filling was added at the end of the ESEEM data to increase the total number of points to 4K; and (5) numerical Fourier transformation was performed to obtain an absolute value spectrum.

Quantum Chemical Computations. All calculations were performed for molecules in vacuo by using the gradient-corrected density functional theory (DFT) method as implemented in the Gaussian 98 package of programs.[13] The three-parameter hybrid exchange functional from Becke,[14] in combination with the correlation functional of Lee et al.,[15] was used throughout this work in unrestricted-spin (UB3LYP) calculations.[16] The standard 6-31++G** basis set was used for the geometry optimizations, whereas the EPR-II and EPR-III basis sets were used for subsequent single-point calculations of spin densities and isotropic and anisotropic hyperfine coupling constants. Note that the EPR-II and EPR-III basis sets of Barone[17−19] are specially intended for the computation of hyperfine coupling constants by DFT methods and reproduce hyperfine coupling parameters accurately for various second-row atoms. In our calculations, the $\langle S^2\rangle$ expectation values range from 0.7545 to 0.7549, before spin projection and annihilation corrections. These $\langle S^2\rangle$ expectation values are very close to the exact one (0.75) for a doublet; therefore, spin contamination of the wave function was negligible.

Theory: ESEEM Simulations

A recent, computationally efficient, exact calculation of ESEEM for nuclei with spin $I = 1$ was used for the simulations.[20,21] The normalized signal intensity at the stimulated echo maximum is given by a sum of signals belonging to the two electron-spin manifolds α and β:

$$V(T+2\tau) = \prod_r V_{r,\alpha} + \prod_r V_{r,\beta} \tag{1}$$

The index r refers to nuclei coupled to the unpaired electron, and the index $q = \alpha$ or β refers to the electron spin eigenstate. By combining results from the two above references, one can write each factor in eq 1 in the form

$$V_{r,q} = \sum_{i,j,k,l,m,n} \exp\{\iota T(\Omega_{q,n} - \Omega_{q,k}) + \iota\tau(\Omega_{\alpha,i} - \Omega_{\alpha,l} + \Omega_{\beta,m} - \Omega_{\beta,j})\}\mathrm{Tr}[\hat{P}_{\alpha,i}\hat{P}_{\beta,j}\hat{P}_{q,k}\hat{P}_{\alpha,l}\hat{P}_{\beta,m}\hat{P}_{q,n}] \tag{2}$$

For simplicity, the index r is omitted on the right-hand side of eq 2, $\Omega_{q,s}$ is the sth eigenvalue of the rth nucleus sub-Hamiltonian in electron-spin manifold q, and $\hat{P}_{q,s}$ is the projection operator onto this eigenstate. If there is no degeneracy in the spectrum of the sub-Hamiltonian $\hat{H}_q$, then the projection operators are given by

$$\hat{P}_{q,n} = \prod_{j\neq n} \frac{\hat{H}_q - \Omega_{q,j}}{\Omega_{q,n} - \Omega_{q,j}} \tag{3}$$

The sub-Hamiltonian for nuclear spin $I \geq {}^1/_2$ in the principal axis system (X, Y, Z) of the quadrupole interaction tensor is

$$\hat{H}_q = \kappa[(3\hat{I}_Z^2 - I(I+1)) + \eta(\hat{I}_X^2 - \hat{I}_Y^2)] + \vec{D}_q\cdot\vec{I} \tag{4}$$

where κ and η are the strength of the quadrupolar coupling and its asymmetry parameter, respectively, and $\vec{D}_q$ is the effective magnetic field for the nuclear spin when the electron spin is in eigenstate q. All quantities with dimensions are in units of angular frequency. The effective field at the nucleus is the sum of the external magnetic field and the hyperfine field. By generalizing relations (eqs 13 and 14) from Maryasov and Bowman[21] to anisotropic hyperfine interactions, one can write

$$\vec{D}_q = \omega_I \vec{k}_z + m_{S,q}\vec{A} \tag{5}$$

where ω_I is the nuclear Larmor frequency, $\vec{k}_z$ is a unit vector along the external magnetic field (z axis in the laboratory frame), and $m_{S,q}$ is the electron spin eigenvalue for eigenstate q ($m_{S,q} = \pm 1/2$). The hyperfine field $\vec{A}$ is given by

$$\vec{A} = \vec{k}_z \vec{\vec{A}} \tag{6}$$

where $\vec{\vec{A}}$ is the electron−nuclear hyperfine interaction tensor.

For nuclear spin $I = 1$, the three eigenvalues of $\hat{H}_q$ in eq 4 may be calculated as suggested by Muha[22,23] (see also ref 21):

$$\Omega_{q,j} = \left(\frac{4|p_q|}{3}\right)^{1/2} \cos\left[\frac{\lambda_q + 2\pi j}{3}\right] \qquad \text{for } j = 0, 1, 2 \tag{7}$$

and

$$\cos \lambda_q = \frac{g_q}{2}\left(\frac{3}{|p_q|}\right)^{3/2} \tag{8}$$

where

$$p_q = -\frac{1}{2}\mathrm{Tr}(H_q^2) = -[D_q^2 + \kappa^2(3 + \eta^2)] \tag{9}$$

and

$$g_q = \frac{1}{3}\mathrm{Tr}(H_q^3) = -\vec{D}_q \vec{Q} \vec{D}_q - 2\kappa^3(1 - \eta^2) \tag{10}$$

The quadrupole tensor is diagonal in its principal axis system, with principal values of $(1 - \eta)\kappa$, $(1 + \eta)\kappa$, and -2κ.

Results

Water penetration into bilayer membranes of DPPC with and without equimolar cholesterol was studied by D_2O modulation in the ESEEM spectra of phosphatidylcholines that were spin labeled systematically down the *sn*-2 chain (*n*-PCSL). In addition to the D_2O modulation, higher-frequency modulation was also observed from protons in the lipid matrix.

To assign the deuterium ESEEM spectra, quantum chemical calculations were performed on the unpaired spin densities for water (D_2O) hydrogen bonded to the spin-labeled nitroxide. ESEEM spectra were then simulated by using hyperfine tensors obtained from these spin densities for H-bonded water and by using classical dipolar (and quadrupolar) calculations for the non-H-bonded waters.

Electron Spin−Echo Envelope Modulation. Figure 1 shows experimental stimulated echo time-domain patterns and the corresponding absolute value ESEEM spectra for the two outermost label positions 4-PCSL and 14-PCSL in DPPC bilayers with (a, c) and without (b, d) equimolar cholesterol. The time-domain patterns are shown in the upper panels of each vertical pair and are normalized by dividing by the average relaxation decay, as described in Materials and Methods. (For a discussion of the correctness of this procedure in quantitative modulation-amplitude analysis, see text below). The interpulse separation, τ, between the first and second pulses was set equal to 168 ns to maximize the deuterium and proton modulations simultaneously in each case. Components are seen in the ESEEM spectra of 4-PCSL (lower of each pair) that are centered around the deuterium Larmor frequency at ca. 2.6 MHz and around that of protons at 14.6 MHz. The amplitude of the deuterium ESEEM spectrum is greater for bilayers of DPPC that contain cholesterol than for those without cholesterol. For 14-PCSL, the nitroxide of which is situated deeper in the bilayer, the deuterium spectrum is almost completely absent. Note that both the deuterium and the proton spectra consist of a sharp component superimposed on a broader background component.

Figure 2 shows the dependence on the spin-label position, n, of the maximum amplitudes of the deuterium (upper panel) and proton (lower panels) ESEEM spectra for DPPC bilayers with and without cholesterol. The amplitude of the lines was measured as the spectral density at 2.2 and 14.6 MHz for deuterium and protons, respectively. The error bars in Figure 2 reflect the noise in the spectra from DPPC alone. For cholesterol-containing samples, the noise in the spectra is smaller than the size of the points in the Figure. The amplitudes of both the deuterium and the proton ESEEM spectra display a sharp change at an intermediate chain position. For deuterium, the modulation amplitude decreases on proceeding deeper into the membrane, whereas for protons the amplitude increases. In DPPC bilayers containing cholesterol, the maximum change occurs at chain position $n = 7-9$. In bilayers of DPPC alone, the maximum change occurs somewhat deeper in the bilayer, around $n = 10-11$.

To obtain deuterium modulation patterns undisturbed by proton modulation, measurements were also performed with an interpulse spacing of $\tau = 204$ ns, which corresponds to the "blind spot" in the stimulated echo for protons.[24] The upper panels in Figure 3 show the normalized modulation patterns for 4-PCSL in DPPC bilayers (a) with and (b) without equimolar cholesterol. High-frequency proton modulation is essentially absent (cf. Figure 1a and b). Corresponding ESEEM spectra are shown in the lower panels of Figure 3. From this, one can see that the deuterium line consists of a broad line with width ca. 2.5 MHz and shoulders at ca. 4 MHz and a narrow Pake doublet with a separation of ∼0.15 MHz and shoulders at ca. 0.4 MHz.

To analyze the correlation between the amplitudes of the broad and narrow deuterium ESEEM components, spectral densities at two positions, 2.6 and 2.2 MHz, respectively, were measured. Amplitudes of the broad and narrow lines were then obtained as follows:

$$I_{\mathrm{narrow}} = \mathrm{Int}(2.2\ \mathrm{MHz}) - \mathrm{Int}(2.6\ \mathrm{MHz})$$

$$I_{\mathrm{broad}} = \mathrm{Int}(2.6\ \mathrm{MHz}) - \mathrm{Int}(\mathrm{background})$$

The two diagnostic positions correspond to the maximum amplitudes of the two deuterium components (Figure 3). Int(background) was taken as the mean value of Int(2.2 MHz) for the 10, 11, 12, 13, and 14th positions in cholesterol-containing bilayers and for 13, 14, and 16th positions for DPPC alone, where the deuterium signal is absent (Figure 2). Figure 4 gives plots of I_{broad} versus I_{narrow} for samples with and without cholesterol. The amplitudes of the broad and narrow deuterium components are seen to correlate for the different spin-labeled positions in both membranes. The dependence is approximately linear but with a tendency toward nonlinearity at the highest amplitudes.

Quantum Chemical Calculations. It is known that a nitroxide can form two strong hydrogen bonds via the N−O radical moiety.[25−27] Water molecules most probably bind to the sp^2 orbital of the oxygen from the N−O fragment. Therefore, the starting point for the geometrical optimization was water molecule(s) situated near the $N-O_{nitr}$ radical fragment, with the $O_{w1}-D$ bond lying along the $D-O_{nitr}$ direction, the angle $D-O_{nitr}-N = 120°$, and $D-O_{nitr} = 2$ Å (cf. Figure 5).

Quantum chemical calculations were made for three structures, with two water molecules that we denote by W_2R (Figure

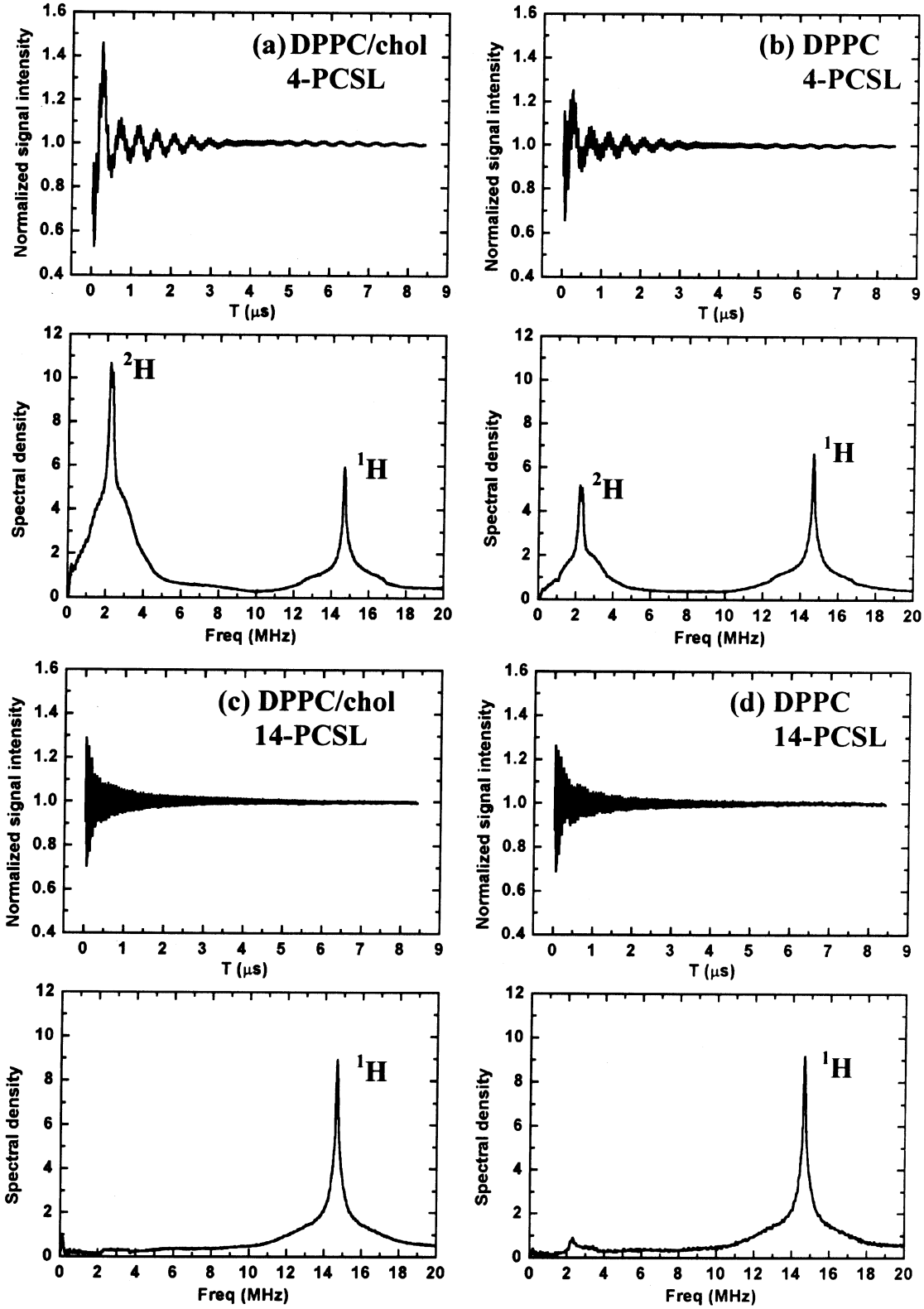

Figure 1. Experimental normalized electron spin−echo decay curves (upper of each vertical pair) and the corresponding Fourier transform ESEEM spectra (lower of each vertical pair) for spin-labeled phosphatidylcholines (*n*-PCSL) in DPPC membranes with and without cholesterol that are hydrated in D_2O. Electron spin−echoes were recorded with an interpulse spacing of $\tau = 168$ ns and are corrected for the electron T_2 decay as described in Materials and Methods. (a) 4-PCSL in a DPPC/cholesterol 1:1 mol/mol mixture. (b) 4-PCSL in DPPC alone. (c) 14-PCSL in a DPPC/cholesterol 1:1 mol/mol mixture. (d) 14-PCSL in DPPC alone.

5a and b) and two structures with one water molecule in two opposite positions, $^{L}W_1R$ and $^{R}W_1R$ (Figure 5c and d). The parameters of the energy-optimized geometry for complexes W_2R, $^{L}W_1R$, and $^{R}W_1R$ are given in Table 1. The hyperfine coupling parameters were obtained for protons and then recalculated for deuterons according to the ratio of their g_n factors (viz., $g_H/g_D = 6.514$). The results of these calculations with the EPR-III basis set are given in Table 2.

Table 3 presents the hyperfine coupling parameters calculated with different basis sets for deuterium D_1 in the W_2R complex.

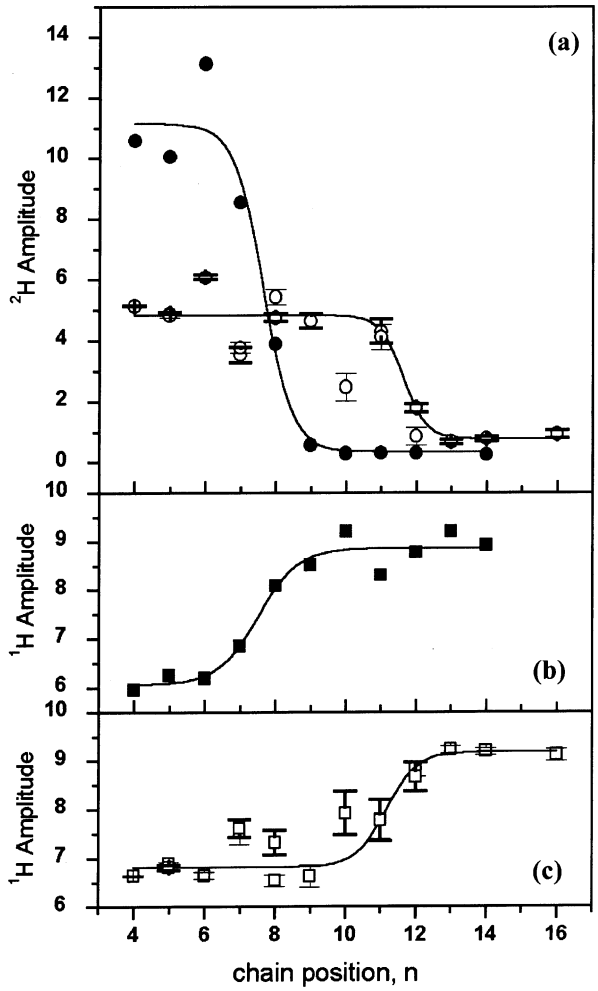

Figure 2. Dependence on spin-label position, *n*, of the ESEEM spectral amplitudes (Figure 1) for DPPC bilayers with (●, ■) and without (○, □) 1:1 mol/mol cholesterol. Solid lines are nonlinear, least-squares fits to eq 11. (a) Amplitude of the deuterium line given as the spectral density at 2.2 MHz. Fitting parameters $n_{o,D} = 7.6 \pm 0.2$ (11.6 ± 0.3), $\lambda_D = 0.4 \pm 0.1$ (0.3 ± 0.2), $I_{1,D} = 11.1 \pm 0.6$ (4.8 ± 0.3), and $I_{2,D} = 0.3 \pm 0.4$ (0.3 ± 0.2) for samples with (without) cholesterol. Amplitude of the proton line given as the spectral density at 14.6 MHz for bilayers (b) with and (c) without cholesterol. Fitting parameters: $n_{o,H} = 8.9 \pm 0.1$ (11.2 ± 0.3) and $\lambda_H = 0.6 \pm 0.2$ (0.4 ± 0.3) for samples with (without) cholesterol.

One can see from these data that the deviation of the results for different basis sets is within 5%. Using the smaller basis set 6-31G* (i.e., without diffuse functions and p functions on the hydrogens) for geometry optimization also gives deviations in the same range (data not shown). These results show that the required parameters are not very sensitive to improvements in the basis set, although the deviations do not reflect the absolute accuracy of these calculations.

The largest basis set among others used for the calculation of hyperfine coupling parameters was EPR-III (a triple-ζ basis set including diffuse functions, double d polarizations, a single set of f-polarization functions, and an enhanced s part). It is expected that the results for this basis set are the most accurate, so they were used for the calculation of the ESEEM that is given below. Also, the relative orientations of the hyperfine coupling tensors were taken in account. (See below.)

The data of Table 3 show that the anisotropic dipole coupling parameters for the D_1 and D_3 nuclei in the W_2R complex and for the D_1 nucleus in the ^RW_1R and ^LW_1R complexes are very close to axial symmetry. Such a situation can be expected when the extent of electron delocalization is much less than the distance to the nucleus. However, this is obviously not the case because the unpaired electron on the nitroxide is equally distributed between the p orbitals of the oxygen and nitrogen atoms, so the extent of delocalization is comparable to the distance between the oxygen and the closest deuterium nucleus. Consequently, it was interesting to estimate the effective distance between the nucleus and the electron, neglecting the small deviation from axial symmetry. Taking A_{ZZ} for the D_1 nucleus in the ^RW_1R structure and using the point-dipole approximation, one obtains a distance of 2.35 Å, which lies between the distances of 1.88 and 2.75 Å to the oxygen and nitrogen, respectively.

Simulation of ESEEM. Several simplifications were introduced into the calculated models. The asymmetry parameter η of the nuclear quadrupole interaction was taken to be equal to zero instead of the experimental value of 0.1. Nuclear quadrupole interaction parameters were taken from the literature.[28−30] The largest component of the quadrupolar tensor is $e^2Qq = 0.215$ MHz, directed along the O−D bond of the water molecule. Figure 5b shows that the geometry of the water molecules and N−O radical fragment is very close to planar. Moreover, the *X* and *Z* principal directions of the hyperfine coupling tensors of all deuterium nuclei lie almost in the same plane (data not shown). Therefore, because all deviations from planar geometry are less than 10°, they were neglected in our calculations. The simplified geometry that was used for the ESEEM calculation is shown in Figure 6, where $\psi_1 = 105°$ and $\psi_2 = 22°$. Note that both H-bonded (D_1 and D_3) and non-H-bonded (D_2 and D_4) nuclei of the D_2O molecules are included in the calculation.

The results of time-domain calculations for H-bonded D_2O molecules are shown in the upper panels of Figures 7a−c. These refer to the W_2R, ^LW_1R, and $^RW_1$ complexes, respectively. A unit baseline has been added to these data for consistency with the relaxation-corrected experimental results. An interpulse delay of $\tau = 204$ ns was used in the calculations in order to compare with the time-domain experimental results in the absence of proton modulation (i.e., Figure 3). Absolute value Fourier transform spectra obtained from the time-domain calculations in the same way as for the experimental ESEEM spectra are given in the lower panels of Figure 7a−c. The spectra for the single water-molecule complexes, ^LW_1R and $^RW_1$, are qualitatively and quantitatively similar. The line shape of the double water-molecule complex, W_2R, is similar to those of the single-water complexes, and the spectral intensity is twice that of the latter. In each case, the line shapes of the calculated spectra closely resemble those of the broad component in the experimental spectra of Figure 3.

The calculation of the ESEEM from the D nuclei of more distant water molecules that do not participate in strong H bonding with the N−O radical was undertaken by using the approach developed by Shubin and Dikanov.[31,32] This method assumes that the hyperfine interaction and nuclear quadrupole interaction are weak compared with the nuclear Zeeman interaction. For the deuterium nuclear quadrupole interaction in D_2O, this is always the case, and for the hyperfine interaction, it restricts the electron−nuclear separation to values greater than 3.5 Å. The geometrical model consists of *N* deuterium nuclei distributed uniformly on the surface of a sphere of radius *R*. Mutual orientations of the nuclei are assumed to be uncorrelated, which is reasonable in our case. Additional averaging was also performed for the relative orientations of the hyperfine and quadrupole tensors.

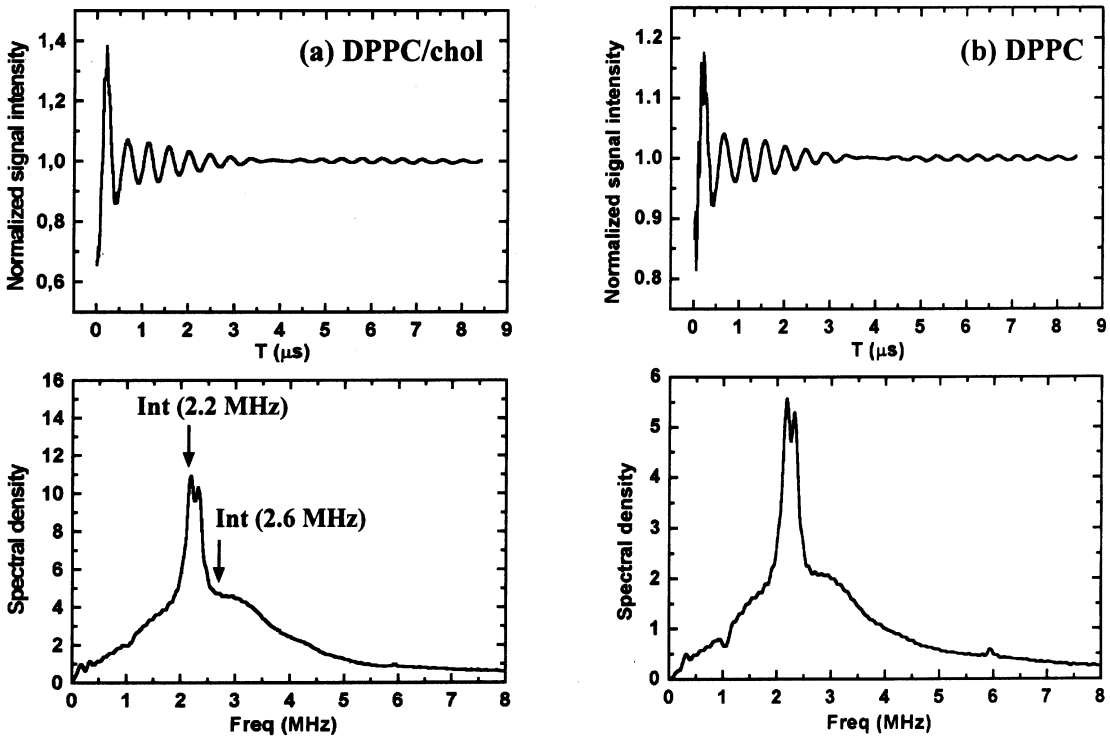

Figure 3. Experimental normalized electron spin−echo decay curves (upper of each pair) and corresponding ESEEM spectra (lower of each pair) from 4-PCSL in (a) bilayers of DPPC/cholesterol 1:1 mol/mol and (b) bilayers of DPPC alone. Electron spin−echoes were recorded with an interpulse spacing of $\tau = 204$ ns to suppress proton modulation. Note that the vertical scales in a and b are different.

TABLE 1: Bond Lengths, Angles, and Dihedral Angles for the DFT-Optimized Geometry of NO−Water Complexes[a]

	W_2R	$^{L}W_1R$	$^{R}W_1R$
NO_{nitr}	1.282	1.278	1.279
$O_{nitr}D_1$	1.899	1.873	1.876
$O_{nitr}D_3$	1.901		
$O_{nitr}O_{w1}$	2.861	2.838	2.842
$O_{nitr}O_{w2}$	2.864		
$D_3O_{nitr}D_1$	115.4°		
$NO_{nitr}D_1$	122.4°	121.2°	121.1°
$O_{nitr}D_1O_{w1}$	168.2°	168.7°	169.3°
$O_{nitr}D_3O_{w2}$	168.7°		
$NO_{nitr}D_1D_2$	152.9°	165.0°	164.5°
$NO_{nitr}D_3D_4$	153.4°		

[a] Bond distances are in Å. Bond angles and dihedral angles are in degrees. For atom numbering, see Figure 5.

TABLE 2: ^{2}H Hyperfine Tensors of NO−D_2O Complexes Calculated with the 6-31++g Basis Set for Geometry Optimization and the EPR-III Basis Set for Hyperfine Parameters**

		isotropic contact	anisotropic dipole coupling (MHz)		
complex	nucleus	coupling (MHz)	A_{XX}	A_{YY}	A_{ZZ}
W_2R	D_1	0.027	−0.876	−0.813	1.689
	D_2	−0.017	−0.202	−0.201	0.403
	D_3	−0.005	−0.891	−0.844	1.735
	D_4	−0.022	−0.209	−0.200	0.409
$^{L}W_1R$	D_1	0.027	−0.948	−0.869	1.816
	D_2	−0.017	−0.211	−0.208	0.419
$^{R}W_1R$	D_1	−0.003	−0.960	−0.897	1.857
	D_2	−0.021	−0.217	−0.207	0.423

Figure 7d shows the results of simulations for more distant water molecules, with a fixed value of $R = 5$ Å. The effective number of nuclei, $N = 12$, was obtained by fitting the intensity of the narrow component in the spectrum of 4-PCSL in DPPC bilayers containing 50 mol % cholesterol (Figure 3a). It is seen that, in this way, the shape, width, and splitting of the narrow component in the experimental spectrum are reasonably well reproduced by the simulation. The values of R and N used to fit the narrow-line intensity are, however, not unique. One can take a smaller value of R and a smaller number N or vice versa and obtain the same intensity, according to the dependence of the modulation depth on dipolar strength that is given by $I \approx N/R^6$. Moreover, for $R > 4.5$ Å, varying R and N in this way does not change the line shape or line width because the line shape is determined predominantly by the quadrupole interaction (that also causes the line splitting) of the deuterium nuclei in the D_2O molecule, and this remains essentially constant.

TABLE 3: ^{2}H Hyperfine Tensors Calculated for Deuterium D_1 in the W_2R Complex by Using Different Basis Sets[a]

basis sets		isotropic contact	anisotropic dipole coupling (MHz)		
geometry optimization	hyperfine parameters	coupling (MHz)	A_{XX}	A_{YY}	A_{ZZ}
6-31++g**	6-31++g**	0.021	−0.879	−0.820	1.700
	EPR-II	0.030	−0.885	−0.835	1.720
	EPR-III	0.027	−0.876	−0.813	1.689

[a] The 6-31++g** basis was used throughout for geometry optimization.

It should be mentioned that the relaxation-decay correction used here suffers from potential nonlinearity in the measured modulation amplitude about the unit normalization level. This is because the constant level to which the modulation pattern is normalized depends somewhat on the modulation amplitude itself. Moreover, modulation from other nuclei (e.g., proton modulation) also shifts this level and therefore might distort the linearity of the normalization procedure. However, all other possibilities, such as normalization to the initial value (at $T = 0$) or to the maximum signal intensity, are influenced more strongly by the modulation depth itself (because of the evolution of the spin system during the fixed τ period between the first and second pulses); additionally, they are much more susceptible to noise because only a single point is taken into account. The method adopted here is, therefore, that best suited for quantita-

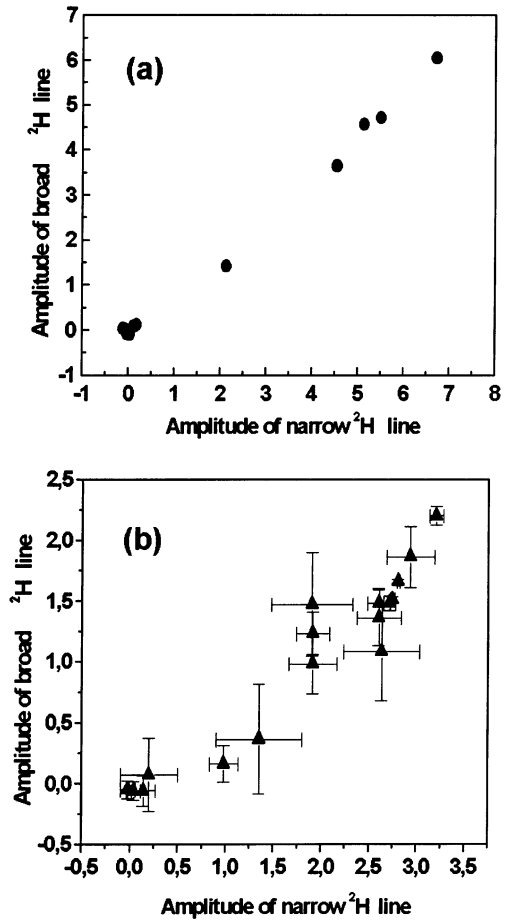

Figure 4. Correlation between the amplitudes of the broad and narrow components in the deuterium (D_2O) ESEEM spectra of the *n*-PCSL spin labels (a) in bilayers of DPPC/cholesterol 1:1 mol/mol and (b) in bilayers of DPPC alone.

tive analysis of ESEEM data; furthermore, because the origins of the nonlinearity are well understood, the extent of nonlinearity can be predicted and estimated.

Discussion

Three-pulse stimulated echo spectroscopy allows resolution of the sharp and broad components in the ^{2}H-ESEEM spectra from lipid spin labels in membranes (see lower panels of Figure 3a and b for 4-PCSL). Simulations based on quantum chemical (DFT) calculations demonstrate that the broad ^{2}H-ESEEM component arises from D_2O molecules that are hydrogen bonded to the spin-labeled nitroxide (compare lower panels of Figure 3a and b with those of Figure 7a and b or c). The deuterium nuclei D_2 and D_4, which do not participate in H bonding, are more remote from the N−O group but still contribute only to the broad component (Figure 7a−c). The narrow component in the experimental ^{2}H-ESEEM spectra therefore reflects water molecules that are free in the membrane and are not H bonded to the spin label. This assignment is confirmed by the ESEEM simulation that is presented in Figure 7d. The amplitude of the modulation from such "matrix" molecules is known to depend linearly on their concentration.[11,33,34]

Transmembrane Profiles. The two D_2O ESEEM components display similar dependences on the position of the spin label in the *sn*-2 chain of the lipid (Figure 4)**.** Measurements of the overall intensity, as given in Figure 2a, are therefore able to establish the transmembrane profile of water penetration. These present, direct measurements of intramembrane water concentration can be compared with previous, more indirect measurements that used spin-label ^{14}N hyperfine splittings and *g* values.[4,5]

The positional profiles of the D_2O ESEEM intensity shown in Figure 2a have approximately sigmoidal shapes that are similar to those found previously for the transmembrane polarity profiles established from isotropic spin-labeled hyperfine couplings.[4] The solid lines that are given in Figure 2 represent fits to the ESEEM intensities, *I*, using the Boltzmann sigmoidal form that has already been employed to characterize the polarity profiles

$$I(n) = \frac{I_1 - I_2}{1 + e^{(n - n_o)/\lambda}} + I_2 \qquad (11)$$

where I_1 and I_2 are the limiting values of *I* at the polar headgroup and terminal methyl ends of the chain, respectively, n_o is the value of *n* at the point of the maximum gradient, corresponding to $I(n_o) = (I_1 + I_2)/2$, and λ is an exponential decay length. The significance of eq 11 is that it corresponds to a two-compartment distribution between outer ($n < n_o$) and inner ($n > n_o$) regions of the membrane in which the free energy of transfer, $(n - n_o)k_BT/\lambda$, increases linearly with the distance, $n - n_o$, from the dividing plane. The fitting parameters in Figure 2a are $n_{o,D} = 7.6 \pm 0.2$ (11.6 ± 0.3) and $\lambda_D = 0.4 \pm 0.1$ (0.3 ± 0.2) for the midpoint and transition width, respectively, for DPPC membranes with (without) cholesterol. Compared with isotropic ^{14}N hyperfine splittings measured in fluid membranes,[4] the transition region between the outer regions of high ^{2}H-ESEEM intensity and the inner regions of low ^{2}H-ESEEM intensity is steeper, characterized by smaller values of λ (0.3−0.4 compared with 0.8). This is a feature of frozen (as opposed to fluid) membranes that is shared with transmembrane profiles derived from high-field ESR measurements of spin-label g_{xx} values and A_{zz} hyperfine splittings at low temperature.[5] For cholesterol-containing DPPC membranes, the transition point ($n_o \approx 8$) of the ^{2}H-ESEEM profile is comparable to that found in fluid membranes ($n_o \approx 9$).[4] However, the shift of the transition midpoint in membranes of DPPC without cholesterol is to higher values ($n_o \approx 11$) in frozen membranes, whereas it is to slightly lower values ($n_o \approx 8$) in fluid membranes.[4] The ^{2}H-ESEEM measurements given in Figure 2a are in agreement with the previous polarity measurements in fluid membranes in that the effect of cholesterol is to increase water concentration in the outer regions of the membrane ($n < 8$) presumably by increasing the separation of the phospholipid headgroups.[4] However, the water concentration in the middle of the frozen membranes is reduced to zero for DPPC bilayers with cholesterol and very close to zero for bilayers without cholesterol (Figure 2a), whereas there is an appreciable nonvanishing water concentration at the bilayer midplane in fluid membranes without cholesterol.[4] Again, this is a feature of frozen membranes that is found also in high-field ESR measurements at low temperature.[5] The present direct observation of intramembrane water therefore fully supports previous interpretations of transmembrane polarity profiles that were determined by more indirect spin-label ESR methods.

Plots b and c of Figure 2 give the profiles of the proton ESEEM intensities for DPPC bilayers with and without cholesterol, respectively. These ^{1}H-ESEEM intensities arise from the matrix protons attached to the lipid chains of the membrane and are directly proportional to the average proton density in the vicinity of the spin label. Because they differ for different spin-labeled positions in the membrane, they must reflect the

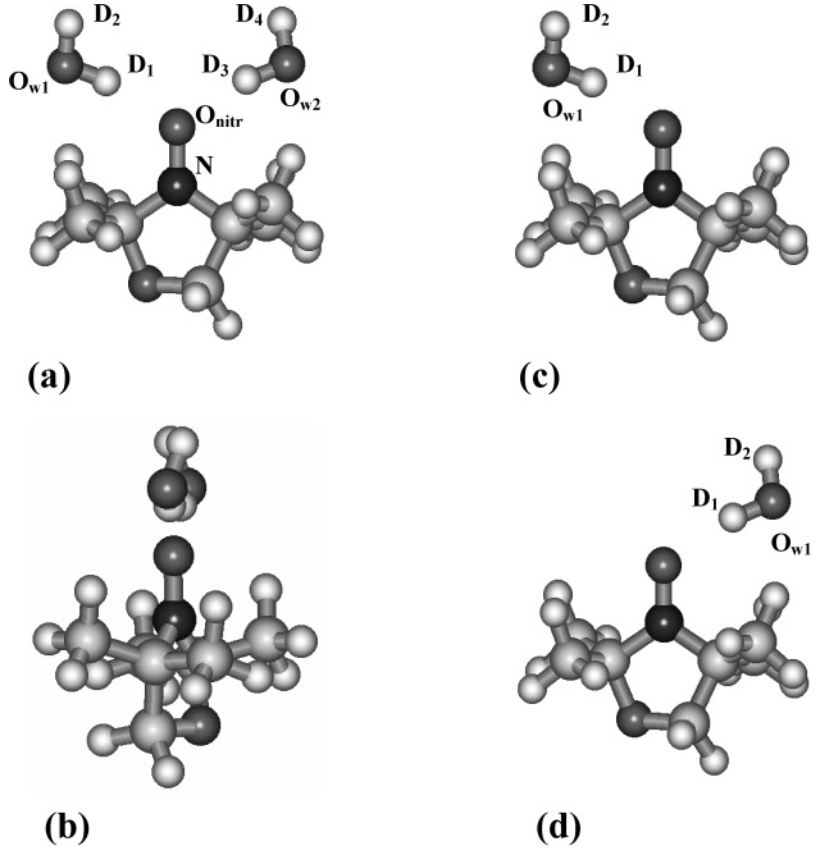

Figure 5. Optimized geometry and atom labeling for the adduct between one or two water molecules and an oxazolidine nitroxide. (a) Complex W_2R with two waters, (b) side view of W_2R, (c) complex $^{L}W_1R$ with one water on the left, and (d) complex $^{R}W_1R$ with one water on the right.

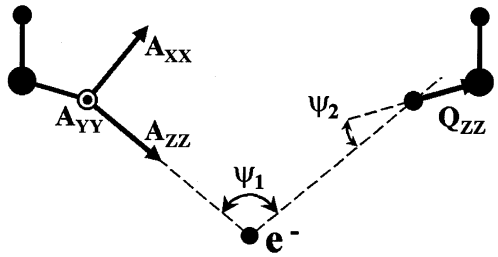

Figure 6. Simplified geometry used for the ESEEM calculation. The orientations of the principal axes of the ^{2}H hyperfine and quadrupole tensors are shown.

local intermolecular chain-packing density. As noted previously, the ^{1}H-ESEEM intensities have profiles similar to those of the accompanying D_2O-modulation intensities (cf. Figure 2a). Correspondingly, the midpoints and widths of the sigmoidal fits are very similar to those of the D_2O intensities: $n_{o,H} = 7.5 \pm 0.2$ and $\lambda_H = 0.6 \pm 0.2$ for DPPC + 50 mol % cholesterol, and $n_{o,H} = 11.2 \pm 0.3$ and $\lambda_H = 0.4 \pm 0.3$ for DPPC alone. Even allowing for the chemically increased proton concentration at the terminal methyl groups, it seems that the average chain-packing density is greater at the middle of the membrane than in the regions of the chain that are closer to the lipid headgroups. This correlates rather well with the D_2O penetration profiles: the water concentration is reduced very strongly in the regions of higher chain-packing density at the middle of the membrane. In regions where water penetration is appreciable, the chains are less densely packed. Possibly, the upper parts of the chain are less tightly packed than are the chain ends because of less optimum packing of the bulky lipid headgroups in frozen hydrated membranes.

Hydrogen Bonding Equilibria. Hydrogen bonding of D_2O to the nitroxide is of interest not only for the interpretation of spin-label ESR measurements of environmental polarity[6,35,36] but also more generally for the interaction of water with the transmembrane domains of integral proteins. On energetic grounds, it is expected that H bonding of water to endogeneous acceptors will be favored in hydrophobic environments, such as the interior of membranes. The correlation between the ^{2}H-ESEEM amplitudes of the narrow and broad spectral components in Figure 4 indicates that the H-bonding equilibrium is frozen in and that the spectral intensities therefore can be treated by using the law of mass action.

Both the local symmetry and the optimized geometries in Table 1 suggest that the binding of single water molecules at the left site and at the right site of the nitroxide (Figures 5c and d) will be energetically equivalent. The successive association of one and two water molecules (W) with the N−O radical (R) can then be depicted by the following local equilibria at the depth in the membrane at which the spin label is situated:

$$R + W \overset{K_1}{\longleftrightarrow} W_1R$$

and

$$W_1R + W \overset{K_2}{\longleftrightarrow} W_2R$$

where K_1 and K_2 are the association constants for the binding of the first and second water molecules, respectively. If the binding of the second water molecule is not strongly affected by the binding of the first water molecule, then K_1 and K_2 are related simply by statistical factors to the intrinsic binding constant, K, for binding to an isolated single site.[37] In terms of the intrinsic single-site binding constant, the concentration of free sites for binding the first water molecule is 2[R], and that

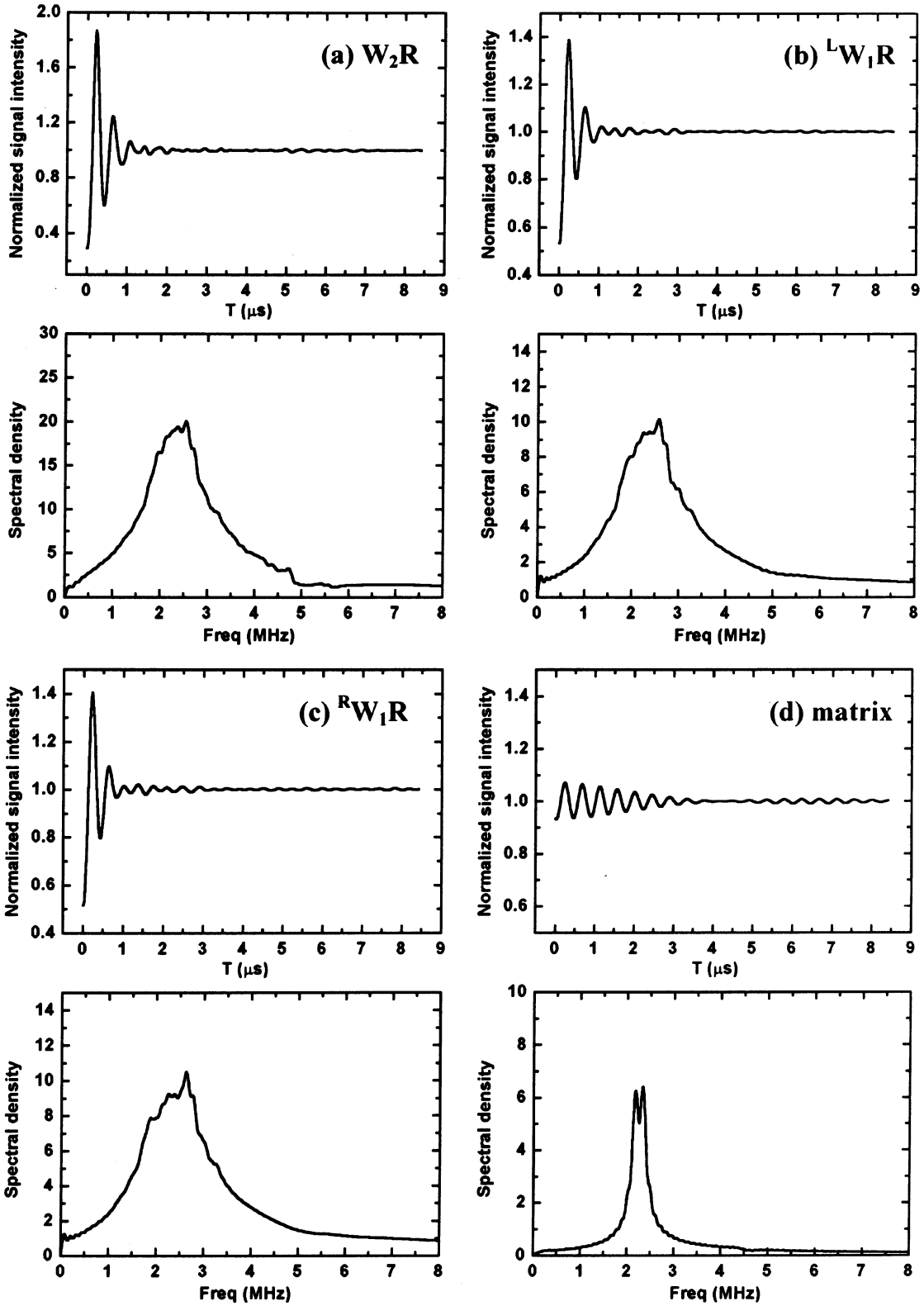

Figure 7. Simulation of electron spin−echo curves (upper of each vertical pair) and ESEEM spectra (lower of each vertical pair) for (a) W_2R, (b) $^{L}W_1R$, and (c) $^{R}W_1R$ complexes and (d) for matrix nuclei with $N = 12$ and $R = 5$ Å. The echo delay is $\tau = 204$ ns for each calculated pattern.

for the dissociation of the second water molecule is $[W_1R]/2$ (i.e., $K_1 = 2K$ and $K_2 = {}^{K}/_{2}$). Conservation of the number of spin labels requires that

$$[R]_o = [R] + [W_1R] + [W_2R] \qquad (12)$$

where $[R]_o$ is the total concentration of spin labels. The concentrations of the H-bonded species, $[W_1R]$ and $[W_2R]$, then can be obtained from the law of mass action, together with eq 12.

If I_o is the ^{2}H-ESEEM intensity for a single D_2O molecule bound (permanently) to the nitroxide (i.e., for complex $^{L}W_1R$ or $^{R}W_1R$), then it is to be expected that the ^{2}H-ESEEM intensity of two D_2O molecules bound permanently in the W_2R complex is $2I_o$. This is seen directly by comparing Figure 7a for W_2R with Figure 7b for $^{L}W_1R$ or with Figure 7c for $^{R}W_2R$. The

normalized intensity of the broad ^{2}H-ESEEM component, under equilibrium conditions for H bonding, is therefore given by

$$\frac{I_{\text{broad}}}{I_o} = \frac{[W_1R]}{[R]_o} + \frac{2[W_2R]}{[R]_o} \tag{13}$$

From eq 12, together with the law of mass action, eq 13 then yields

$$\frac{I_{\text{broad}}}{I_o} = \frac{2K[W]}{1 + K[W]} \tag{14}$$

This equation gives the dependence of the amplitude of the broad line in the deuterium ESEEM spectrum on the local water concentration. From the simulations given in Figure 7b and c, the intrinsic intensity for a singly bonded D_2O molecule is given by $I_o \approx 9.5$. It will be noted that this estimate relies directly on the ability of DFT calculations to predict absolute ESEEM intensities.

Taking the experimental values of $I_{\text{broad}} \approx 4.5$ and 2.1 for 4-PCSL in DPPC + 50 mol % cholesterol and in DPPC alone from Figure 3a and b, one obtains values of $K[W] \approx 0.31$ and 0.12, respectively, from eq 14. This quantity gives the relative populations of doubly and singly H-bonded nitroxides directly: $[W_2R]/[W_1R] = K[W]/2$. The fraction of spin labels with a single water molecule bound is given by

$$\frac{[W_1R]}{[R]_o} = \frac{2}{(1/K[W]) + 2 + K[W]} \tag{15}$$

This yields values for the fraction that is singly H-bonded of $[W_1R]/[R]_o \approx 0.36$ and 0.20 for 4-PCSL in membranes of DPPC + 50 mol % cholesterol and of DPPC alone, respectively. The corresponding fractions for two bound water molecules are $[W_2R]/[R]_o \approx 0.06$ and 0.01, respectively. Of course, these values all fall progressively to zero at the position of 14-PCSL, close to the middle of the membrane (see Figures 1c and d and 2a).

The above estimates suggest the presence of heterogeneity in the number of water molecules that are H-bonded to 4-PCSL. Some spin labels in the region of the chain closer to the lipid headgroups (i.e., for $n < 8$) still have no bonded water molecules, others have one bonded water molecule, and a smaller fraction have two bonded water molecules. This conclusion is consistent with the finding that the polarity-sensitive g_{xx} feature in the high-field ESR spectra of spin labels in this chain region displays considerable inhomogeneous broadening relative to that of spin labels located close to the middle of the membrane.[5] Quantum chemical calculations of different types predict shifts in g_{xx} of ca. -4×10^{-4} for one hydrogen bond.[38,39] The measured difference between spin labels with $n < 8$ and with $n > 8$ in membranes of DPPC + 40 mol % cholesterol is $\Delta g_{xx} \approx -6 \times 10^{-4}$,[5] but this includes contributions from differences in polarity that are not directly attributable to hydrogen bonding.[35] Therefore, the binding estimates made from ^{2}H-ESEEM data are reasonably consistent with the g shifts measured by high-field ESR. Conversely, this gives some degree of confidence in the estimates of absolute ^{2}H-ESEEM intensities derived from the DFT calculations.

The equilibrium constant for hydrogen bonding of water to nitroxides in a hydrophobic environment is not known with certainty, but experimental estimates from other systems suggest values of $K \geq 1\ M^{-1}$.[36] Adopting this value yields estimates of $[W] \leq 0.3$ and 0.1 M for the local water concentration in the region of 4-PCSL in DPPC membranes with and without cholesterol, respectively. Estimates from isotropic hyperfine splittings using this value for the K yield: $[W] \leq 1.3$ and 1.0 M for the upper part of the chain in fluid membranes of DPPC with and without 50 mol % cholesterol, respectively.[36] Differences could reflect differing H-bond strengths of H_2O and D_2O as well as differences in the lipid phase. It is possible that the above estimates for K may be too low because molecular dynamics simulations of water penetration yield considerably lower intramembrane water concentrations.[40]

Free Intramembrane Water. Information on the water penetration in lipid membranes, undisturbed by the spin label, comes from the free water concentration, [W]. (Note that the spin-label concentration is only 1 mol % and the bulk water concentration in the aqueous phase, $[W]_o = 55.5$ M, is far greater than the intramembrane water concentration.) The free water concentration in the membrane is reflected directly by the amplitude of the narrow ^{2}H-ESEEM peak. However, as already explained, the ESEEM simulations for the narrow peak are not unique. The model involving N_{eff} water molecules at fixed distance R_{eff} does not reflect the true local concentration of free water. To obtain the latter, it is necessary to integrate N/R^6 over the free water distribution in the local environment of the spin label. In the plateau region, occupied by 4-PCSL to 7-PCSL at the top of the chains, the number density of free water molecules can be assumed to have a constant average value $\bar{n}_{W,1}$. The amplitude of the ^{2}H-ESEEM spectrum is then proportional to the following expression:[9,41]

$$\langle k_M \rangle \propto \bar{n}_{W,1}\left[\int_0^{z_o}\int_{r_{WL}}^{\infty} \frac{2\pi\rho\, d\rho\, dz}{[(z - z_{SL})^2 + \rho^2]^3} + \int_0^{z_{SL} - r_{WL}}\int_0^{r_{WL}} \frac{2\pi\rho\, d\rho\, dz}{[(z - z_{SL})^2 + \rho^2]^3} + \int_{z_{SL}+r_{WL}}^{z_o}\int_0^{r_{WL}} \frac{2\pi\rho\, d\rho\, dz}{[(z - z_{SL})^2 + \rho^2]^3}\right] \tag{16}$$

where z_{SL} ($= n \times 1.47$ Å) is the vertical spin-label position around the middle of region 1, z_o ($= n_o \times 1.47$ Å) corresponds to chain position n_o at the transition midpoint in the profile, and r_{WL} is the distance of closest approach of free water molecules to the spin label. The expression on the right of eq 16 is quantitatively equivalent to $N_{\text{eff}}/R_{\text{eff}}^6$. The last two terms correspond to the vertical regions immediately above and immediately below the spin label. Performing the double integrations in eq 16, we calculate the reciprocal number density of water molecules from

$$\bar{n}_{W,1}^{-1} = \frac{\pi}{12 r_{WL}^3}\left(\frac{R_{\text{eff}}^6}{N_{\text{eff}}}\right)\left[7 + \frac{3\pi}{2} - 2r_{WL}^3\left(\frac{1}{(z_o - z_{SL})^3} + \frac{1}{z_{SL}^3}\right)\right] \tag{17}$$

The value of r_{WL} is an effective quantity because it depends on the molecular details in the immediate vicinity of the spin label. It involves all water molecules that are in direct contact with the nitroxide but are not in the correct orientation for H bonding. In the H-bonding direction, r_{WL} is, however, much larger. We will take a value of $r_{WL} = 1.9$ Å that is equal to the closer $O_{nitr}D$ distance in Table 1. The smallest value could be even less for some orientations because the unpaired electron density is centered approximately in the middle of the N−O bond.[42] Also, we add 9 Å to the values of z_{SL} and z_o to allow approximately for water molecules in the headgroup region of the membrane. This correction contributes only ca. 10% to the

value of N_{eff}/R_{eff}^6. With $N_{eff} = 12$ and $R_{eff} = 5$ Å, eq 17 then leads to $\bar{n}_{W,1} = 1.7 \times 10^{21}$ cm^{-3}, which corresponds to an intrabilayer water concentration in the outer membrane regions of [W] = 2.9 M. This value is considerably higher than the free water concentrations quoted in the previous section. Uncertainties in the present estimate arise from a strong dependence on the exact value of r_{WL} and nonlinearities in the dependence of the ESEEM amplitude on concentration for waters close to the spin label. For comparison with the above water concentrations, the effective concentration of chain CH_2 groups in the interior of a frozen bilayer is ca. 65 M.[43]

Note that water molecules from the other side of the bilayer do not contribute because these make no contribution to the ^{2}H-ESEEM intensity, even at the bilayer center. Also, water molecules from the water layer immediately outside the bilayer are unlikely to contribute greatly because an appreciable $(1/R^3)$ dependence on the distance from the bilayer surface is not observed in the outer plateau region (i.e., in region 1). Direct calculation indicates a contribution of only 1% from the extramembrane water to the value of N_{eff}/R_{eff}^6 for 4-PCSL.

Conclusions

Free and H-bonded water have been resolved in the D_2O ESEEM spectra of lipid chains spin labeled across the width of bilayer membranes. The permeation profiles for water are found to have the sigmoidal, troughlike form that is characteristic of more indirect determinations of intramembrane polarity. Water penetration is therefore a primary contributor to the transmembrane polarity profile and correlates with the lipid packing density that is registered by the ^{1}H-ESEEM from the chain matrix protons. An analysis of the H-bond equilibria within the membrane gives estimates of the local intramembrane concentrations of free water and of the singly and doubly H-bonded nitroxides. In the upper regions of the chains, an appreciable proportion of spin-label NO groups are H bonded to water. This has important general implications for the binding of water to H-bond acceptors (and correspondingly also to H-bond donors) within the membrane interior. For instance, water H-bonded at the intramembranous surface of integral proteins could potentiate the diffusive water permeation pathway through the lipid membrane.

The results have direct relevance for the understanding of the transport properties of biological membranes and for the energetics of insertion of proteins.

Acknowledgment. We thank Frau B. Angerstein for the synthesis of spin-labeled phospholipids. R.B., L.S., and D.M. are members of the COST D22 Action of the European Union. D.A.E. and S.A.D. thank INFM and CRDF (no. NO-008-x1) for financial support. This work was supported by a grant from the project CIPE-Cluster MIA26-P5BWP3.

References and Notes

(1) Cevc, G.; Marsh, D. *Phospholipid Bilayers: Physical Principles and Models*; Wiley-Interscience: New York, 1987.
(2) Griffith, O. H.; Dehlinger, P. J.; Van, S. P. *J. Membr. Biol.* **1974**, *15*, 159−192.
(3) Subczynski, W. K.; Wisniewska, A.; Yin, J. J.; Hyde, J. S.; Kusumi, A. *Biochemistry* **1994**, *33*, 7670−7681.
(4) Marsh, D. *Proc. Natl. Acad. Sci. U.S.A.* **2001**, *98*, 7777−7782.
(5) Kurad, D.; Jeschke, G.; Marsh, D. *Biophys. J.* **2003**, *85*, 1025−1033.
(6) Marsh, D.; Kurad, D.; Livshits, V. A. *Chem. Phys. Lipids* **2002**, *116*, 93−114.
(7) Hiff, T.; Kevan, L. *J. Phys. Chem.* **1989**, *93*, 1572−1575.
(8) Kurshev, V. V.; Kevan, L. *J. Phys. Chem.* **1995**, *99*, 10616−10620.
(9) Bartucci, R.; Guzzi, R.; Marsh, D.; Sportelli, L. *Biophys. J.* **2003**, *84*, 1025−1030.
(10) Noethig-Laslo, V.; Cevc, P.; Arcon, D.; Sentjurc, M. *Origins Life Evol. Biosphere* **2003**, *34*, 237−242.
(11) Dikanov, S. A.; Tsvetkov, Y. D. *Electron Spin−Echo Envelope Modulation (ESEEM) Spectroscopy*; CRC Press: Boca Raton, FL, 1992.
(12) Marsh, D.; Watts, A. Spin-Labeling and Lipid−Protein Interactions in Membranes. In *Lipid−Protein Interactions*; Jost, P. C., Griffith, O. H., Eds.; Wiley-Interscience: New York, 1982; Vol. 2, pp 53−126.
(13) Frisch, M. J.; Trucks, G. W.; Schlegel, H. B.; Scuseria, G. E.; Robb, M. A.; Cheeseman, J. R.; Zakrzewski, V. G.; Montgomery, J. A., Jr.; Stratmann, R. E.; Burant, J. C.; Dapprich, S.; Millam, J. M.; Daniels, A. D.; Kudin, K. N.; Strain, M. C.; Farkas, O.; Tomasi, J.; Barone, V.; Cossi, M.; Cammi, R.; Mennucci, B.; Pomelli, C.; Adamo, C.; Clifford, S.; Ochterski, J.; Petersson, G. A.; Ayala, P. Y.; Cui, Q.; Morokuma, K.; Malick, D. K.; Rabuck, A. D.; Raghavachari, K.; Foresman, J. B.; Cioslowski, J.; Ortiz, J. V.; Stefanov, B. B.; Liu, G.; Liashenko, A.; Piskorz, P.; Komaromi, I.; Gomperts, R.; Martin, R. L.; Fox, D. J.; Keith, T.; Al-Laham, M. A.; Peng, C. Y.; Nanayakkara, A.; Gonzalez, C.; Challacombe, M.; Gill, P. M. W.; Johnson, B. G.; Chen, W.; Wong, M. W.; Andres, J. L.; Head-Gordon, M.; Replogle, E. S.; Pople, J. A. *Gaussian 98*, revision A.11; Gaussian, Inc.: Pittsburgh, PA, 2001.
(14) Becke, A. D. *Phys. Rev. A* **1988**, *38*, 3098−3100.
(15) Lee, C. T.; Yang, W. T.; Parr, R. G. *Phys. Rev. B* **1988**, *37*, 785−789.
(16) Becke, A. D. *J. Chem. Phys.* **1993**, *98*, 5648−5652.
(17) Adamo, C.; Barone, V.; Fortunelli, A. *J. Chem. Phys.* **1995**, *102*, 384−393.
(18) Barone, V. In *Recent Advances in Density Functional Methods*; Chong, D. P., Ed.; World Scientific: Singapore, 1995; Part 1.
(19) Rega, N.; Cossi, M.; Barone, V. *J. Chem. Phys.* **1996**, *105*, 11060−11067.
(20) Maryasov, A. G.; Bowman, M. K.; Tsvetkov, Y. D. *Appl. Magn. Reson.* **2002**, *23*, 211−233.
(21) Maryasov, A. G.; Bowman, M. K. *J. Phys. Chem. B* **2004**, *108*, 9412−9420.
(22) Muha, G. M. *J. Chem. Phys.* **1980**, *73*, 4139−4140.
(23) Muha, G. M. *J. Magn. Reson.* **1983**, *53*, 85−102.
(24) Schweiger, A.; Jeschke, G. *Principles of Pulse Electron Paramagnetic Resonance*; Oxford University Press: Oxford, U.K., 2001.
(25) Engström, M.; Owenius, R.; Vahtras, O. *Chem. Phys. Lett.* **2001**, *338*, 407−413.
(26) Symons, M. C. R.; Pena-Nunez, A. S. *J. Chem. Soc., Faraday Trans. 1* **1985**, *81*, 2421−2435.
(27) Improta, R.; Scalmani, G.; Barone, V. *′Chem. Phys. Lett.* **2001**, *336*, 349−356.
(28) Blinc, R.; Hadzi, D. *Nature* **1966**, *212*, 1307−1309.
(29) Chiba, T. *J. Chem. Phys.* **1964**, *41*, 1352−1358.
(30) Semin, G. K.; Babushkina, T. A.; Yakobson, G. G. *Application of Nuclear Quadrupole Resonance in Chemistry*; Chemistry Press: Leningrad, 1972.
(31) Shubin, A. A.; Dikanov, S. A. *J. Magn. Reson.* **1983**, *52*, 1−12.
(32) Shubin, A. A.; Dikanov S. A. *J. Magn. Reson.* **1985**, *64*, 185−193.
(33) Dikanov, S. A.; Tsvetkov, Y. D. *Zh. Strukt. Khim.* **1979**, *20*, 824−829.
(34) Dikanov, S. A.; Astashkin, A. V.; Tsvetkov, Y. D. *Zh. Strukt. Khim.* **1982**, *23*, 11.
(35) Marsh, D. *J. Magn. Reson.* **2002**, *157*, 114−118.
(36) Marsh, D. *Eur. Biophys. J.* **2002**, *31*, 559−562.
(37) Tanford, C. *Physical Chemistry of Macromolecules*; Wiley: New York, 1961.
(38) Owenius, R.; Engström, M.; Lindgren, M.; Huber, M. *J. Phys. Chem. A* **2001**, *105*, 10967−10977.
(39) Plato, M.; Steinhoff, H. J.; Wegener, C.; Törring, J. T.; Savitsky, A.; Möbius, K. *Mol. Phys.* **2002**, *100*, 3711−3721.
(40) Marrink, S. J.; Berendsen, H. J. C. *J. Phys. Chem.* **1996**, *100*, 16279−16738.
(41) Livshits, V. A.; Dzikovski, B. G.; Marsh, D. *J. Magn. Reson.* **2001**, *148*, 221−237.
(42) Makinen, M. W.; Mustafi, D.; Kasa, S. ENDOR of Spin Labels for Structure Determination: From Small Molecules to Enzyme Reaction Intermediates. In *Spin Labeling. The Next Millenium*; Berliner, L. J., Ed.; Plenum Press: New York, 1998; pp 181−249.
(43) Marsh, D. *Handbook of Lipid Bilayers*; CRC Press: Boca Raton, FL, 1990.